Biology   Faculty Publications & Research

2016

Osteopontin ablation ameliorates muscular dystrophy by shifting macrophages to a proregenerative phenotype

Sylvia Vetrone

Joana Capote

Irina Kramerova

Leonel Martinez

Elisabeth R. Barton

See next page for additional authors

Authors

Sylvia Vetrone, Joana Capote, Irina Kramerova, Leonel Martinez, Elisabeth R. Barton, H. Lee Sweeney, M. Carrie Miceli, and Melissa J. Spencer

Osteopontin ablation ameliorates muscular dystrophy by shifting macrophages to a pro-regenerative phenotype

Joana Capote,[1,3] Irina Kramerova,[1] Leonel Martinez,[1] Sylvia Vetrone,[1] Elisabeth R. Barton,[6,7] H. Lee Sweeney,[5,7] M. Carrie Miceli,[2,4,7] and Melissa J. Spencer[1,4,7]

[1]Department of Neurology and [2]Department of Microbiology, Immunology, and Molecular Genetics, David Geffen School of Medicine, University of California, Los Angeles, Los Angeles, CA 90095
[3]Molecular, Cellular, and Integrative Physiology Interdepartmental PhD Program, University of California, Los Angeles, Los Angeles, CA 90095
[4]Center for Duchenne Muscular Dystrophy at UCLA, Los Angeles, CA 90095
[5]Department of Pharmacology and Therapeutics, University of Florida, Gainesville, FL 32610
[6]Department of Applied Physiology and Kinesiology, University of Florida, Gainesville, FL 32611
[7]Wellstone Muscular Dystrophy Center, University of Florida, Gainesville, FL 32610

In the degenerative disease Duchenne muscular dystrophy, inflammatory cells enter muscles in response to repetitive muscle damage. Immune factors are required for muscle regeneration, but chronic inflammation creates a profibrotic milieu that exacerbates disease progression. Osteopontin (OPN) is an immunomodulator highly expressed in dystrophic muscles. Ablation of OPN correlates with reduced fibrosis and improved muscle strength as well as reduced natural killer T (NKT) cell counts. Here, we demonstrate that the improved dystrophic phenotype observed with OPN ablation does not result from reductions in NKT cells. OPN ablation skews macrophage polarization toward a pro-regenerative phenotype by reducing M1 and M2a and increasing M2c subsets. These changes are associated with increased expression of pro-regenerative factors insulin-like growth factor 1, leukemia inhibitory factor, and urokinase-type plasminogen activator. Furthermore, altered macrophage polarization correlated with increases in muscle weight and muscle fiber diameter, resulting in long-term improvements in muscle strength and function in mdx mice. These findings suggest that OPN ablation promotes muscle repair via macrophage secretion of pro-myogenic growth factors.

Introduction

Patients with mutations in the *DMD* gene have Duchenne muscular dystrophy (DMD), which is a progressive muscle degenerative disease that leads to loss of skeletal muscle cardiomyopathy and eventual death (Bushby et al., 2010). In DMD, defective dystrophin protein causes muscle membrane fragility, leading to contraction-induced injury caused by high forces on the cell membrane and leading to cycles of muscle fiber degeneration and regeneration (Vetrone et al., 2009; Heydemann et al., 2009). Inflammatory cells invade in response to the repeated waves of damage and repair and release cytokines, which promote pathological fibrosis (Borthwick et al., 2013). Fibrosis leads to loss of mobility and function and has the potential to

interfere with gene and stem cell therapies. Inflammatory cells also secrete promyogenic factors that enable proper myogenic differentiation and are absolutely necessary for successful muscle repair (Cantini et al., 2002; Dumont and Frenette, 2010; Saclier et al., 2013). Thus, modulating the inflammatory cell infiltrate in dystrophic muscle has the potential to target both fibrosis and regeneration and represents a therapeutic target for DMD. Such treatment may attenuate disease and improve the efficacy of other therapies if used in combination.
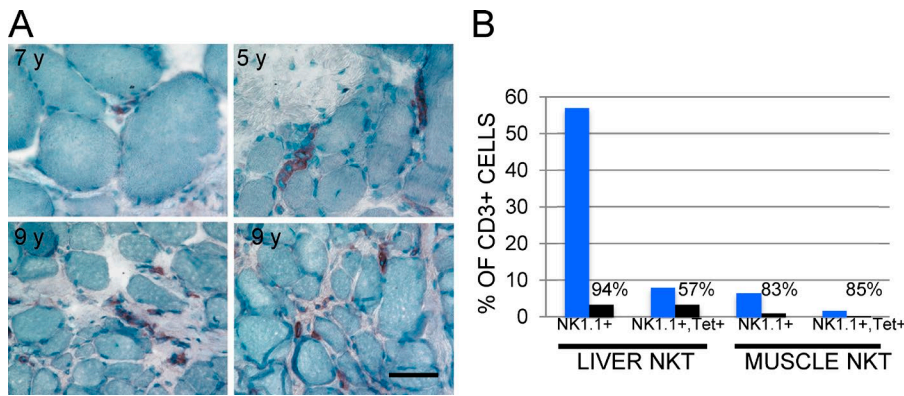
Macrophages are the predominant immune cell type found in the inflammatory infiltrate of human DMD and mdx muscles (McDouall et al., 1990; Wehling et al., 2001). Macrophages that infiltrate dystrophic muscles are a heterogeneous mix of classically (M1) and alternatively (M2) activated types (Villalta et al., 2009; Mann et al., 2011). M1 macrophages are classified as proinflammatory because they express known proinflammatory mediators (tumor necrosis factor, interleukin [IL]-1β, and IL-6)

The Rockefeller University Press $30.00
J. Cell Biol. Vol. 213 No. 2 275–288
www.jcb.org/cgi/doi/10.1083/jcb.201510086

JCB 275

A

B

% OF CD3+ CELLS

LIVER NKT
NK1.1+ — 94%
NK1.1+,Tet+ — 57%

MUSCLE NKT
NK1.1+ — 83%
NK1.1+,Tet+ — 85%

Figure 1. **NKT cells are observed in muscles from patients with Duchenne muscular dystrophy and are depleted from mdx muscle and liver by GM1 treatment.** (A) Cross sections from DMD biopsies were immunostained with an antibody against Vα24, the invariant chain of human NKT cells. Positive staining appears red, and counterstain with hematoxylin labels the nuclei dark blue and the muscle tissue light blue. Bar, 100 µm. (B) Quantification of liver and muscle NKT cells from GM1- or PBS-treated animals. The graph shows a representative experiment in which each bar represents the values obtained from pooled muscles isolated from three mice injected with PBS (blue bars) and three mice injected with GM1 (black bars). The plot illustrates the frequency of CD3+ cells that coexpress either [NK1.1] or [NK1.1+ CD1d-tetramer]. Numbers shown represent the amount of depletion attained by GM1 treatment compared with PBS controls.

and reactive nitrogen and oxygen intermediates (Mantovani et al., 2007; Novak and Koh, 2013; Liu et al., 2014; Rigamonti et al., 2014). M1 macrophages have also been shown to promote myoblast proliferation and collagen production in fibroblasts in vitro (Song et al., 2000; Cantini et al., 2002). The alternatively activated M2 macrophages, on the other hand, are a more heterogeneous group: M2 macrophages can be subdivided into M2a, M2b, and M2c macrophages (Liu et al., 2014; Rigamonti et al., 2014; Wermuth and Jimenez, 2015). M2a macrophages are believed to be fibrosis promoting (Song et al., 2000; Cantini et al., 2002), whereas M2c macrophages are thought to be deactivating for M1 macrophages and pro-regenerative. Although the markers for M1 macrophages are fairly well defined, the markers to distinguish different subpopulations of M2 macrophages are less so, particularly M2c.

Osteopontin (OPN), encoded by the *SPP1* gene, is the most highly up-regulated transcript in dystrophic muscles (Haslett et al., 2002; Porter et al., 2002). OPN is a multifunctional protein that binds to a vast array of cell surface receptors, (primarily integrins; Bayless et al., 1998; Casals et al., 2008) to activate diverse signaling pathways including nuclear factor-κB and protein kinase B. Osteopontin activity has been shown to affect diverse cellular processes such as bone remodeling, cell motility, cell adhesion, and cell survival (Das et al., 2005; Nyström et al., 2007; Kahles et al., 2014). Our prior work identified OPN as a potential immunomodulator that regulates fibrosis in the mouse model of DMD (Vetrone et al., 2009). In those studies, OPN ablation correlated with reduced muscle fibrosis, reduced TGF-β, and increased regeneration. Moreover, we found that OPN ablation altered the inflammatory milieu, leading to reductions in several immune cell populations such as natural killer T (NKT) cells and Gr-1+ cells, as well as an increase in FoxP3 mRNA levels (a marker of regulatory T cells). However, the net effect of these changes in immune cell populations and the specific manner in which OPN ablation alters dystrophic disease is not completely understood.

Here we elucidate how changes induced by OPN ablation affect the pathogenesis of dystrophinopathies. The data show that OPN ablation skews dystrophic macrophages toward a pro-regenerative phenotype, leading to improved and sustained muscle mass and strength on long-term functional testing. This investigation provides insight into the role of OPN in dystrophic muscle and further substantiates its value as a therapeutic target for DMD.

Results

Role of NKT cells in the mdx phenotype

Our previous investigations demonstrated modulation of the mdx immune infiltrate after OPN ablation (Vetrone et al., 2009). In those studies, OPN ablation led to a significant decrease in the frequencies of intramuscular NKT and Gr-1+ cells invading mdx muscles (Vetrone et al., 2009). NKT cells are T cells that also express NK cell markers (e.g., NK1.1 or DX5; Godfrey and Kronenberg, 2004). These cells are activated by glycolipids, which are presented in the context of membrane-bound CD1d molecules, akin to the manner in which T cells recognize peptides in the context of major histocompatibility complex (MHC) class I and II. To determine whether these cells are relevant to the human disease, 10 biopsies from DMD boys ranging from 3 to 9 yr of age were examined for evidence of NKT cells within the muscle tissue, by using an antibody against the invariant α chain (Vα24) expressed by human NKT cells. This analysis confirmed that scattered Vα24+ cells were present in the biopsies (Fig. 1 A).

To understand whether changes in NKT populations (such as those observed with OPN ablation) might underlie amelioration of the dystrophic phenotype, we conducted in vivo depletion of NKT cells using an antibody against asialo-GM1, which was injected into mdx mice. Asialo-GM1 is a well-established cell surface ganglioside of NK and NKT cells that is necessary for their complete activation. Treatment with anti–asialo-GM1 has been previously shown to result in a reduction of both cell types (Slifka et al., 2000; Nakagawa et al., 2001; Nakano et al., 2002; Byrne et al., 2004). mdx mice were treated from 1 wk of age until they were assessed for functional and phenotypic features of muscular dystrophy at 4 and 24 wk of age. To verify that treatments were effective in depleting NKT cells, we evaluated intramuscular NKT cells in treated mice, using tetramers of CD1d in conjunction with markers of NK and T cells (Fig. 1 B). Liver NKT cells were examined in parallel as a positive control. The analysis showed that GM1 treatment reduced intramuscular NKT cells (i.e., cells coexpressing CD3+, NK1.1+, and CD1d+ tetramer) by 85% (Fig. 1 B). Tetramer-negative NKT cells (i.e., cells expressing CD3+, NK1.1+, and CD1d−) were also depleted by GM1 treatment, by 83% (Fig. 1 B). In spite of reductions in NK and NKT cells, attenuation of intramuscular fibrosis or other features of the mdx phenotype was not observed at either

the 4- or 24-wk time points (Table 1). Thus, the studies eliminate NKT cells as effectors of the dystrophic phenotype and suggest that the previously observed phenotypic improvements on OPN ablation were not a result of reductions in NKT cells.

Macrophage polarization is altered in the absence of OPN

Our prior studies demonstrated that the frequency of Gr-1^{+} cells (previously used as a Ly6G marker) was significantly reduced in OPN^{−/−}mdx muscles (Vetrone et al., 2009). Because the Gr-1 antibody recognizes both Ly6G (a neutrophil-specific marker) and Ly6C (a pan-granulocyte and macrophage marker) we sought to further explore the Gr-1^{+} cell types affected by OPN ablation. Double-staining of isolated mdx leukocytes with Gr-1 and F4/80 antibodies revealed that neutrophils make up ∼7% of the total CD45^{+} leukocytes at 4 wk and 5 mo of age (Fig. 2 A), which is a smaller percentage of the leukocyte infiltrate than we had previously estimated (Vetrone et al., 2009). However, consistent with our prior results, the frequency of neutrophils was slightly decreased in OPN^{−/−}mdx muscles (Fig. 2 A). Also consistent with our prior results, there was no change in the frequency of F4/80^{+} cells upon OPN ablation. To determine the frequency of eosinophils versus macrophages in the F4/80[+] population, we stained for Siglec F, which is a marker of eosinophils. Eosinophils comprised ∼15% of all F4/80^{+} cells (Fig. 2 B), and their frequency was not altered in the absence of OPN (Fig. 2 B).

Examination of the Ly6C marker on isolated leukocytes revealed a striking shift in its distribution (between Ly6C^{low} vs. Ly6C^{high}) in OPN^{−/−}mdx mice (Fig. 3 A). Because Ly6C levels change from high to low as macrophages undergo polarization (Arnold et al., 2007; Varga et al., 2013; Crane et al., 2014), we reasoned that the altered Ly6C levels might reflect changes in macrophage subtypes. To determine whether the observed shift in Ly6C was caused by a change in macrophage polarization, we examined sorted F4/80^{+} cells from 4- and 8-wk-old mdx mice for expression of Ly6C. To obtain reproducible data, it was necessary to sort the F4/80^{+} cells and then exclude the eosinophils, based on side scatter height (SSC-H) and forward scatter height (FSC-H) gating (Fig. 3 B). The macrophages were subsequently analyzed for Ly6C expression, which revealed the presence of three distinct populations: (a) F4/80[low]Ly6C^{high}; (b) F4/80[medium]Ly6C[medium]; and (c) F4/80[high]Ly6C^{low} (Fig. 3 C). Quantitative evaluation of these macrophage populations showed that the Ly6C^{high} and Ly6C[medium] populations were significantly decreased in the OPN^{−/−}mdx mice, whereas a significant increase was observed in the Ly6C^{low} population in both 4- and 8-wk-old OPN^{−/−}mdx mice (Fig. 4). A similar tendency in skewing of macrophage polarization was also observed in an acute injury model with OPN ablation (Fig. S1). Thus, a consistent skewing of Ly6C was observed on isolated macrophages from OPN^{−/−}mdx mice.

Levels of F4/80 and Ly6C correlate with M1, M2a, and M2c macrophage subtypes

To further characterize the phenotype of the macrophage populations that we observed, we used FACS based on their Ly6C and F4/80 surface expression. After sorting, leukocytes from 4- and 8-wk-old mdx mice were examined for gene expression profiles commonly associated with macrophage subtypes (Fig. 5). The F4/80[low]Ly6C^{high} macrophages displayed high levels of iNOS expression, with very little or no Arg-1, CD206, or CD163 expression, thus resembling M1 macrophages. The other two groups of macrophages, F4/80[medium]Ly6C[medium] and F4/80^{high}Ly6C^{low}, were both Arg-1^{+}, CD206^{+}, and CD163^{+}, with little to no iNOS expression. However, the F4/80[medium]Ly6C[medium] group had the highest Arg-1 expression, suggesting that they resembled the M2a subtype, whereas F4/80[high]Ly6C^{low} showed higher CD206 and CD163 expression and low Arg-1, suggesting that these cells align with the profile of M2c macrophages. Thus, based on these expression profiles, we have defined F4/80[low]Ly6C^{high} macrophages as M1, F4/80[medium]Ly6C[medium] as M2a, and F4/80[high]Ly6C^{low} as M2c. These data reveal that OPN ablation in mdx mice alters macrophage polarization toward decreased M1 and M2a subtypes and increased M2c type macrophages. Overall, the ratios of M1 to M2 are decreased at both 4 and 8 wk of age (Fig. 5 C and Table S1).

OPN is a novel marker of M2c macrophages

We next examined whether OPN is differentially expressed in the three macrophage subtypes. Analysis of OPN expression in the sorted populations demonstrated that M2c macrophages express the highest levels of OPN compared with M1 and M2a subtypes, suggesting that OPN may be a novel and suitable marker for identification of M2c macrophages (Fig. 6). To further characterize the expression of OPN in macrophage populations, we evaluated OPN expression in a macrophage cell line that was induced to polarize according to defined macrophage phenotypes by exposure to specific cytokines. J774A.1

Table 1. **Functional and histological features of dystrophic mice treated with GM1**

| Characteristic	4 wk				6 mo			
	mdx-R.sera		mdx-GM1		mdx-R.sera		mdx-GM1	
	Mean ± SD	n	Mean ± SD	n	Mean ± SD	n	Mean ± SD	n
Body weight, g	11.08 ± 2.2	30	11.61 ± 1.79	29	28.94 ± 4.46	11	29.93 ± 3.9	11
Wire test, seconds on wire	31.83 ± 10.6	23	33.46 ± 13.27	28	18.93 ± 10.76	11	15.6 ± 11.34	11
Creatine kinase, IU/L	25,039 ± 11,620	6	26,851 ± 8,997	6	10,745 ± 4,959	6	11,086 ± 3,789	6
Histopathology								
Quadriceps, % necrotic area	8.04 ± 4.35	6	11.08 ± 5.39	8	3.71 ± 1.27	9	4.82 ± 2.66	9
Diaphragm, % necrotic area	NA	NA	NA	NA	6.69 ± 2.05	6	6.15 ± 2.22	6
NCAM, % positive fibers	5.11 ± 2.3	13	5.91 ± 3.03	12	NA	NA	NA	NA
devMHC, % positive fibers	5.06 ± 1.61	9	6.79 ± 2.93	10	NA	NA	NA	NA

NA, not applicable.
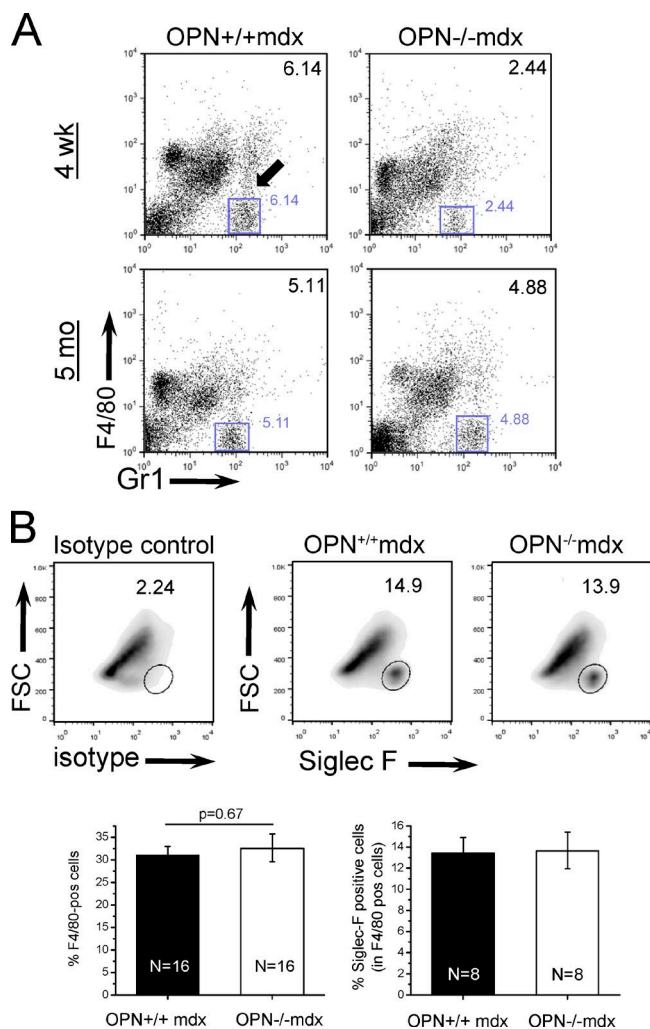
Figure 2. **Analysis of Ly6C+ cells in OPN−/−mdx infiltrates.** (A) Muscle leukocytes were isolated from OPN−/−mdx and OPN+/+mdx muscles, stained for Gr1 and F4/80, and assessed by flow cytometry. FACS plots show F4/80 plotted against Gr1. Cells enclosed by the blue square represent neutrophils. The frequency of neutrophils is indicated in the top right of each quadrant. (B) Analysis of eosinophils was performed by Siglec F staining on sorted F4/80+ cells from OPN+/+mdx and OPN−/−mdx muscles. Circled regions in the FACS plots represent the eosinophil population, and numbers indicate eosinophil frequencies (top). Bottom graphs show the quantification of F4/80+ cell frequency in the total intramuscular leukocyte population (bottom left) and eosinophils in the intramuscular F4/80+ cell population (bottom right). Black bars represent OPN+/+mdx, and white bars represent OPN−/−mdx. Animal numbers are indicated on graphs. P-values were generated by Student's *t* test. Vertical lines represent SEM.

macrophages were exposed to IFNγ, IL-4, or IL-10, and their expression of traditional macrophage polarization markers was assessed: inducible nitric oxide synthase (iNOS) for M1, Arg-1 for M2a, and IL-10 for M2c macrophages (Fig. 7 A). We observed that expression of iNOS, Arg-1, and IL-10 was induced by IFNγ, IL-4, and IL-10 treatment, respectively, suggesting that the macrophages polarized as expected; however, we observed that IL-10 expression was also induced in cells treated with IFNγ, suggesting that IL-10 is not a specific M2c marker (Fig. 7 A). Additionally, we observed that OPN expression was specifically induced in M2c macrophages treated with IL-10, at both the RNA (Fig. 7 C) and protein (Fig. 7 D) levels, suggesting
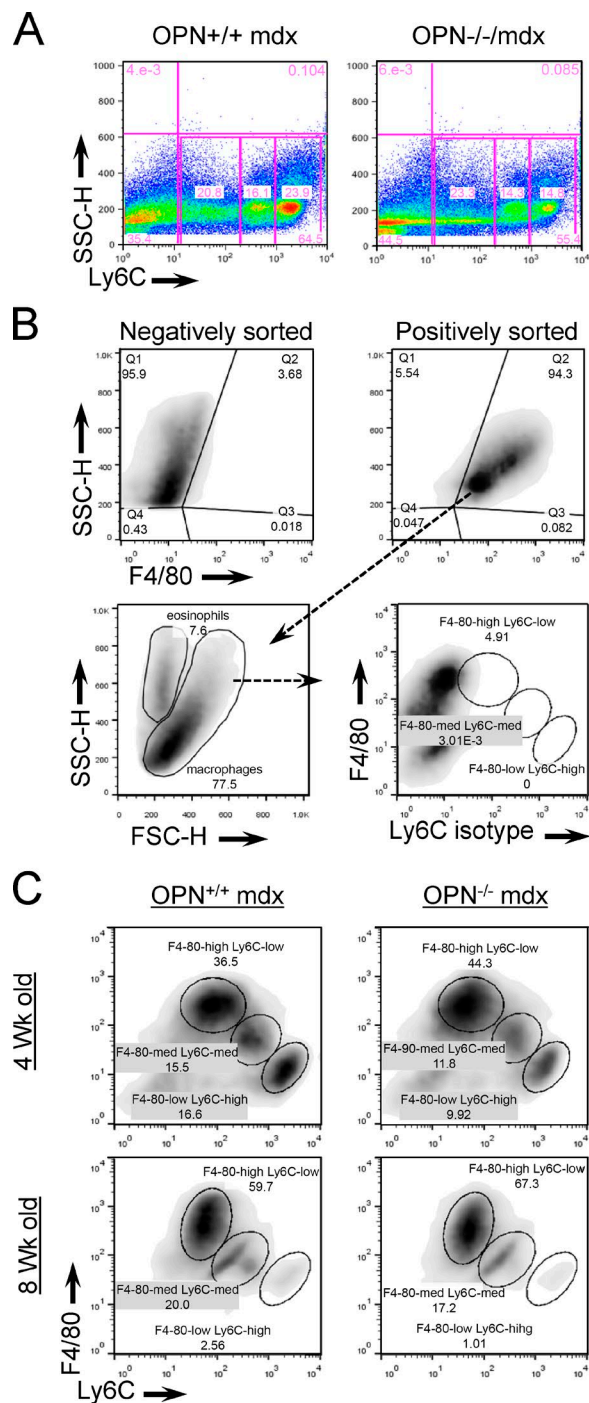
Figure 3. **Evaluation of macrophage polarization by cell sorting and FACS analysis.** (A) Representative FACS plots of muscle-infiltrating leukocytes stained for Ly6C and plotted against SSC for OPN+/+mdx and OPN−/−mdx. (B) Demonstration of the purity of MACS sorting. The top left FACS plot shows F4/80 staining of the negatively sorted population, and the top right FACS plot shows F4/80 staining of the positively sorted population. Positively sorted cells (arrow) were examined by SSC and FSC to isolate macrophages (larger population on the right) from eosinophils (left). The bottom right FACS plot shows Ly6C isotype control staining on the macrophage population used in these studies. (C) Representative FACS plots of MACS-sorted F4/80+ macrophages stained for F4/80 and Ly6C. Circled regions represent distinct macrophage populations. Experiments were done at 4 and 8 wk of age. Quantification of these experiments is shown in Fig. 4.
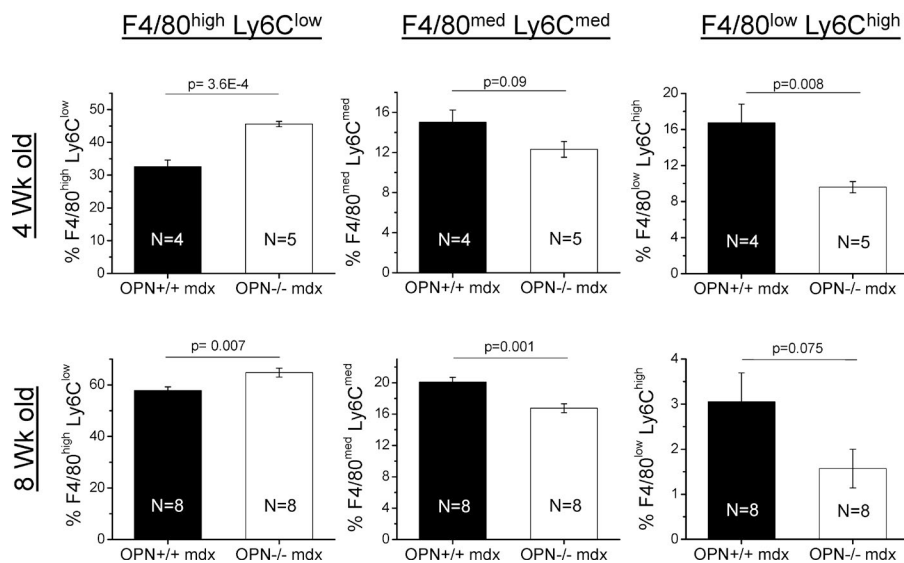
Figure 4. **Macrophage polarization is skewed in OPN⁻/⁻mdx muscles.** Quantification of macrophage subpopulations from MACS-sorted F4/80⁺ macrophages isolated from OPN⁺/⁺mdx and OPN⁻/⁻mdx muscles. Plots depict mean values of pooled data from 4-wk-old (top) and 8-wk-old (bottom) mice, assessed as described in Fig. 3. Vertical lines represent standard errors. Animal numbers are indicated on each bar of the graph. Statistical significance determined by Student's *t* test. P-values are indicated.

that OPN is most highly expressed in this subtype of macrophage. The data show that OPN is a marker that distinguishes M2c macrophages from M1 and M2a types. To our knowledge, this finding suggests that OPN may represent the first specific M2c macrophage marker.

OPN ablation promotes the expression of pro-regenerative factors from mdx macrophages

Because the phenotype of tissue macrophages dictates the manner in which they influence a disease process, we sought to identify the functional outcome of the observed shift in macrophage polarization in the setting of OPN ablation in mdx mice. To this end, we assessed the expression of profibrotic and pro-regenerative factors by RT-PCR on sorted F4/80⁺ cells

isolated from OPN⁻/⁻mdx and OPN⁺/⁺mdx muscles. Based on the previous observations of reduced fibrosis in OPN⁻/⁻mdx muscles (Vetrone et al., 2009), we expected to detect a decrease in profibrotic cytokines such as TGF-β. However, no significant differences were observed in the expression of different profibrotic factors such as fibronectin (Vidal et al., 2008), C-C chemokine ligand 17 (Belperio et al., 2004), and TGF-β (Vidal et al., 2008; Fig. 8 A). On the contrary, OPN⁻/⁻mdx macrophages showed significantly increased expression of pro-regenerative factors, such as insulin-like growth factor 1 (Barton et al., 2002), leukemia inhibitory factor (Hunt et al., 2013), and urokinase plasminogen activator (Suelves et al., 2007; Fig. 8 B). Thus, OPN ablation appears to skew macrophages toward a pro-regenerative macrophage phenotype in dystrophic muscles.
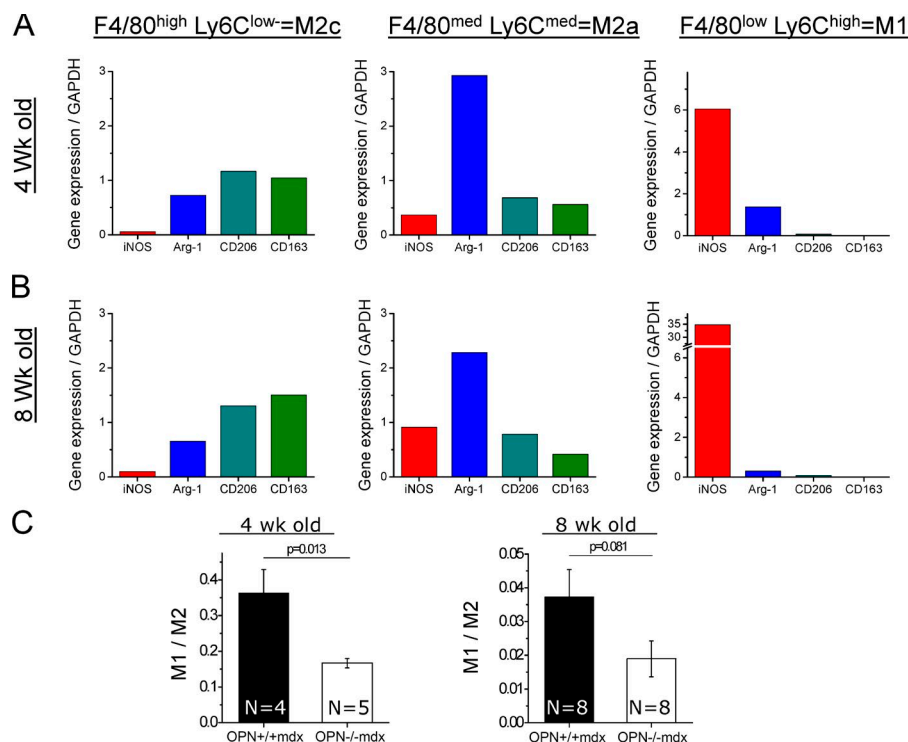
Figure 5. **Levels of F4/80 and Ly6C correlate with M1, M2a, and M2c macrophage subtypes.** Quantitative RT-PCR was used to evaluate mRNA expression of phenotypic markers from sorted macrophage populations isolated from muscles of 4-wk-old (A) or 8-wk-old (B) mice. Macrophage populations were defined and sorted (according to F4/80 and Ly6C levels) from a single sample of pooled muscles collected from six 4-wk-old mice (A) and six 8-wk-old mice (B). Samples were run in triplicate to measure the expression of these genes. All values are expressed relative to GAPDH. (C) Graph of M1 vs M2 ratios at 4 and 8 wk of age. Vertical lines represent SEM.
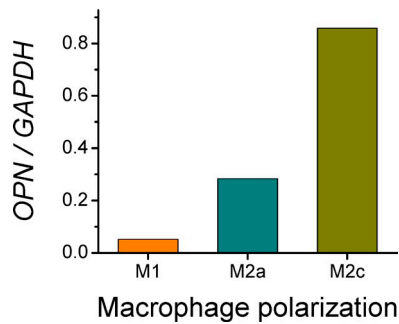
Figure 6. **Assessment of OPN mRNA levels in FACS-sorted macrophage populations.** Graph demonstrates data derived from quantitative RT-PCR of OPN mRNA from sorted macrophage subtypes. Macrophage populations were defined and sorted (according to F4/80 and Ly6C levels) from a single sample of pooled muscles collected from six 8-wk-old mice and characterized as shown in Fig. 5. Expression of OPN was normalized to GAPDH. Samples were run in triplicate to measure the expression of both genes.

## OPN ablation correlates with increased muscle mass and fiber diameter

The observed increase in pro-regenerative growth factors is consistent with our prior study of increased regenerating fibers in OPN$^{-/-}$mdx muscles (Vetrone et al., 2009). To determine whether the observed shift toward a pro-regenerative macrophage phenotype on OPN ablation leads to overall increases in muscle mass, we examined muscle weight and fiber diameter in the two genotypes of mice. Quadriceps muscles were carefully dissected and weighed, and the muscle weight was normalized to tibia length. This analysis showed a significant increase in quadriceps muscle mass at 3 mo, 6 mo, and 1 yr of age (Fig. 9). Extensor digitorum longus (EDL) muscle mass was also significantly increased at 6 mo of age (Fig. 9). Because the EDL is a small muscle with parallel fiber architecture, we also assessed the number of fibers and fiber diameter in this muscle. Although the number of fibers per cross-sectional area did not differ between genotypes, we observed an overall increase in the fiber cross-sectional area in OPN$^{-/-}$mdx EDL. Examination of the distribution of the fiber diameters revealed that the differences were in the smallest and largest fibers, suggesting that two processes were being affected in the OPN$^{-/-}$mdx: muscle regeneration and muscle growth.

OPN ablation induces long-term amelioration of the dystrophic phenotype in mdx mice

To determine whether the improvements in muscle mass that we observed led to long-term consequences for the health and function of dystrophic muscles, we performed noninvasive functional muscle testing and physiological muscle strength tests on OPN$^{-/-}$mdx and OPN$^{+/+}$mdx mice over a long time course. These studies revealed that OPN ablation led to a sustained improvement in muscle strength in dystrophic mice (Fig. 10). OPN$^{-/-}$mdx mice performed better on wire hanging (Fig. 10 A), grip strength (Fig. 10 B), and wire mesh (Fig. 10 C) tests, without large changes in body weight (Fig. 10 D). Physiological testing of single isolated EDL, soleus, and diaphragm muscles from OPN$^{-/-}$mdx mice showed a significant increase in specific force (Fig. 10 E). Moreover, we observed significantly reduced serum creatine kinase (Fig. 10 F) and improved pulmonary function (based on improved minute ventilation and peak expiratory flow as shown in Fig. 10, G–I). Thus, these studies reveal that the pro-regenerative phenotype observed in OPN$^{-/-}$mdx macrophages correlates with long-term improvements in muscle strength and function.

Discussion

In this investigation, we sought to understand the manner in which OPN ablation attenuates the severity of muscular dystrophy using the mdx mouse model. Several leukocyte populations were evaluated as a follow-up to our prior investigation in which we observed changes in NKT and Gr-1$^+$ cells in OPN$^{-/-}$mdx mice (Vetrone et al., 2009). Here we demonstrate that the reduced frequency of NKT cells on OPN ablation (Vetrone et al., 2009) does not contribute to the amelioration of dystrophic pathology: depletion of greater than 80% of NKT cells in mdx muscles did not improve phenotypic features of the disease (Table 1). Thus, our results confirm that these cells are not disease promoting in dystrophinopathies and that reductions in NKT cells do not play a causal role in the improvements that occur in OPN$^{-/-}$mdx mice.
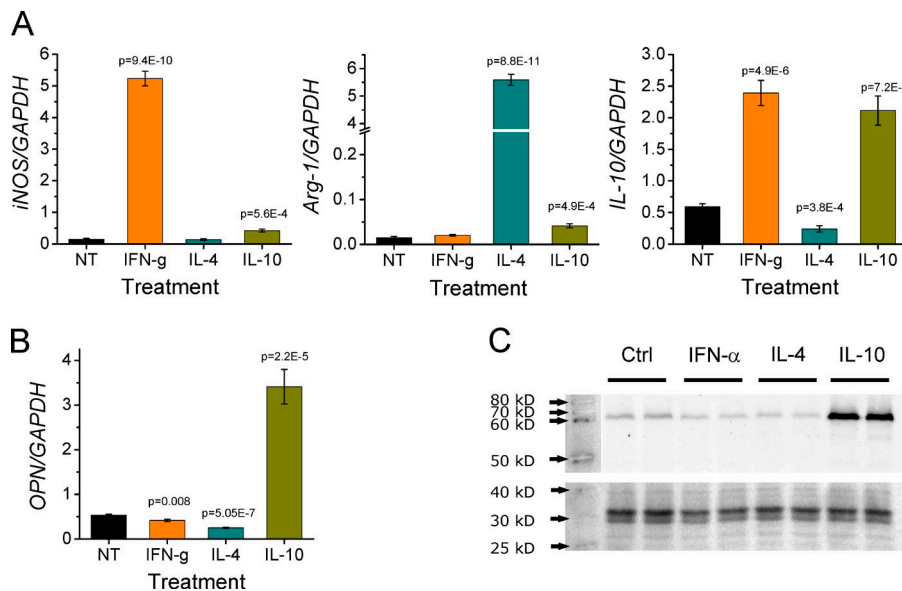
Figure 7. **In vitro polarization of macrophages reveals high expression of OPN in M2c macrophages.** The J774A macrophage cell line was induced to different macrophage subtypes by exposure to polarizing cytokines in vitro to model macrophage polarization. Exposure to IFNγ polarizes to M1, exposure to IL4 polarizes to M2a, and exposure to IL10 polarizes to M2c. NT, not treated. Polarizing treatments are indicated under each bar of the graph. (A) Expression of iNOS (M1), Arg-1 (M2a), and IL-10 (M2c) was assessed by quantitative RT-PCR to confirm macrophage phenotype (top). (B) Quantitative RT-PCR assessment of OPN mRNA expression in polarized macrophages. Each bar in the plots from A and B represents the mean value calculated from six samples collected in three different experiments. (C) Western blot of polarized macrophage extracts reveals high OPN in M2c macrophages. Polarizing cytokines are indicated above the lanes. Vertical bars represent standard error. P-values relative to nontreated cells are indicated based on Student's t test.
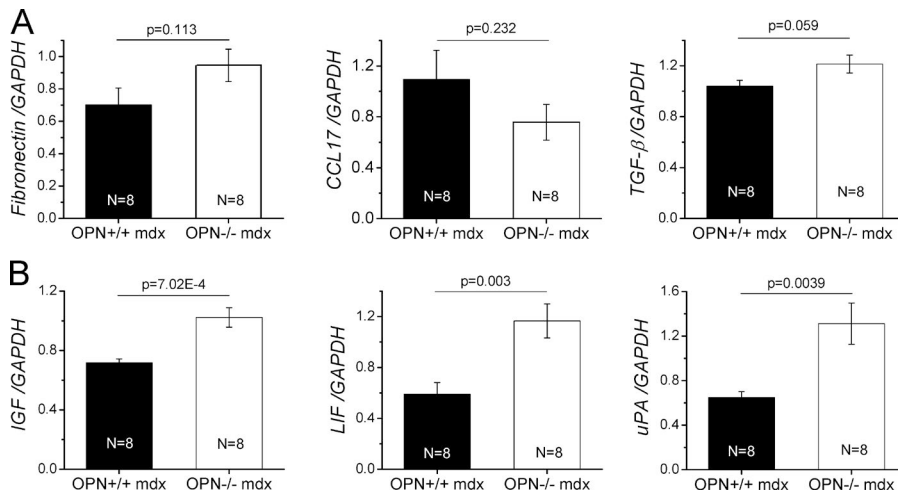
Figure 8. **OPN ablation promotes a pro-re-generative macrophage phenotype.** F4/80+ sorted macrophages were collected from 8-wk-old mice and assessed by quantitative RT-PCR for profibrotic factors fibronectin, C-C chemokine ligand 17 (CCL17), and TGF-β (A) and pro-regenerative factors insulin-like growth factor 1 (IGF), leukemia inhibitory factor (LIF), and urokinase plasminogen activator (uPA). (B) Each sample was collected from a single mouse. The number of samples per experiment is indicated on the bars. Vertical lines indicate SEM. P-values are shown based on Student's t test comparison.

An important finding of this investigation is the role that we revealed for OPN in macrophage polarization in the setting of dystrophinopathy. Shifts in macrophage phenotypes have been previously proposed to influence the course of mdx dystrophy (Villalta et al., 2009, 2011a,b), whereby reductions in IFNγ, iNOS, or C-C chemokine receptor 2 reduce the M1/M2 ratio and attenuate disease (Villalta et al., 2011a; Mojumdar et al., 2014), whereas IL-10 ablation increases the M1/M2 ratio and exacerbates disease (Villalta et al., 2011b). In agreement with the previous findings, we show here that the OPN ablation-induced decrease in the M1/M2 ratio of mdx macrophages improves the dystrophic phenotype and increases muscle mass and strength. In addition, we identify OPN as a potential new marker of M2c macrophages. Our studies show that OPN is more specific than CD163 and IL-10 in identifying the M2c macrophage subtype, both in vivo and in vitro.

The increased muscle strength observed in this investigation is highly likely to be related to the significant increase in macrophage expression of pro-regenerative factors insulin-like growth factor 1 (Barton et al., 2002), leukemia inhibitory factor (Barton et al., 2002; Hunt et al., 2013), and urokinase plasminogen activator (Suelves et al., 2007; Bryer et al., 2008). At the same time, no significant difference was observed in the expression of profibrotic factors such as fibronectin (Vidal et al., 2008; To and Midwood, 2011), C-C chemokine ligand 17 (Belperio et al., 2004; Yogo et al., 2009), and TGF-β (Fig. 8). The increase in pro-regenerative factors agrees with the relative shift toward M2c macrophages that we observed with OPN ablation, because M2c macrophages have been traditionally classified as the pro-regenerative macrophage subtype.

The effect of OPN ablation on macrophage polarization may be direct or indirect. OPN has been previously shown to suppress iNOS and IL-10 expression and induce IL-12, IL-6, tumor necrosis factor, and IL-1β expression in a variety of in vitro macrophage models (Rollo et al., 1996; Rollo and Denhardt, 1996; Ashkar et al., 2000; Koguchi et al., 2002; Weber et al., 2002; Naldini et al., 2006; Gao et al., 2007). Future studies are needed to gain insight into the specific relationship between OPN and macrophage polarization in the context of dystrophic muscles.

We previously observed reductions in TGF-β in muscles of OPN⁻/⁻mdx mice, but the results here reveal that alterations in TGF-β levels are not caused by the observed shift in macrophage polarization. Magnetic-activated cell sorting (MACS) allowed us to more specifically evaluate the cytokine contribution of macrophages to the dystrophic milieu and eliminate macrophages as the source of reduced TGF-β on OPN ablation. This result leaves us without an explanation for why OPN ablation reduces TGF-β levels in dystrophic muscles. OPN biology is complex, and thus intensive studies on isolated cell types will be required to fully elucidate all of the pathways it regulates in dystrophic muscle. OPN binds to a large number of different integrins, as well as to the glycoprotein CD44, and may affect different cell types including fibroblasts (Goodison et al., 1999). OPN can also be retained intracellularly or posttranslationally modified by cleavage, phosphorylation, and glycosylation, thus adding complexity to understanding its role in dystrophy. More studies are necessary to fully understand which of its targets and signaling pathways are involved in DMD.

The changes induced in the macrophage population by OPN ablation correlated with improved muscle strength and function: OPN⁻/⁻mdx mice were stronger than OPN⁺/⁺mdx mice. mdx mice lacking OPN were able to hang 1.2–8 times longer than mdx mice when tested in the wire and mesh tests, at most ages tested. They also had less muscle damage, as shown by a significant decrease in serum creatine kinase levels. Additionally, we showed that OPN ablation in mdx mice improved respiratory function, suggesting that diaphragm muscle pathology is reduced. Although there was a significant improvement in the dystrophic phenotype, OPN ablation does not restore mdx mice muscle strength back to normal (Fig. S2). We anticipate that OPN inhibitors would be beneficial and could be used in combination therapy with other agents to slow disease progression and improve muscle function.

The complex biology of OPN and its multifaceted impact on signaling pathways in different cells types may provide an explanation for conflicting studies about OPN as a disease modifier of DMD. Kyriakides et al. (2011) identified a single nucleotide polymorphism (SNP) in the promoter of the OPN gene (*SPP1*) that correlated with a more severe disease course, compared with the more common haplotype. The SNP is found in the AP1 binding site, very close to the translational start site of the protein. In that initial study, patients with the GG/TG SNP lost ambulation sooner than patients with the TT SNPs and expressed 2.7-fold higher levels of OPN. Although a few subsequent studies on this modifier were inconclusive, follow-up study confirmed the modifier effect, but interestingly, the effect was observed only in steroid-treated patients (Bello
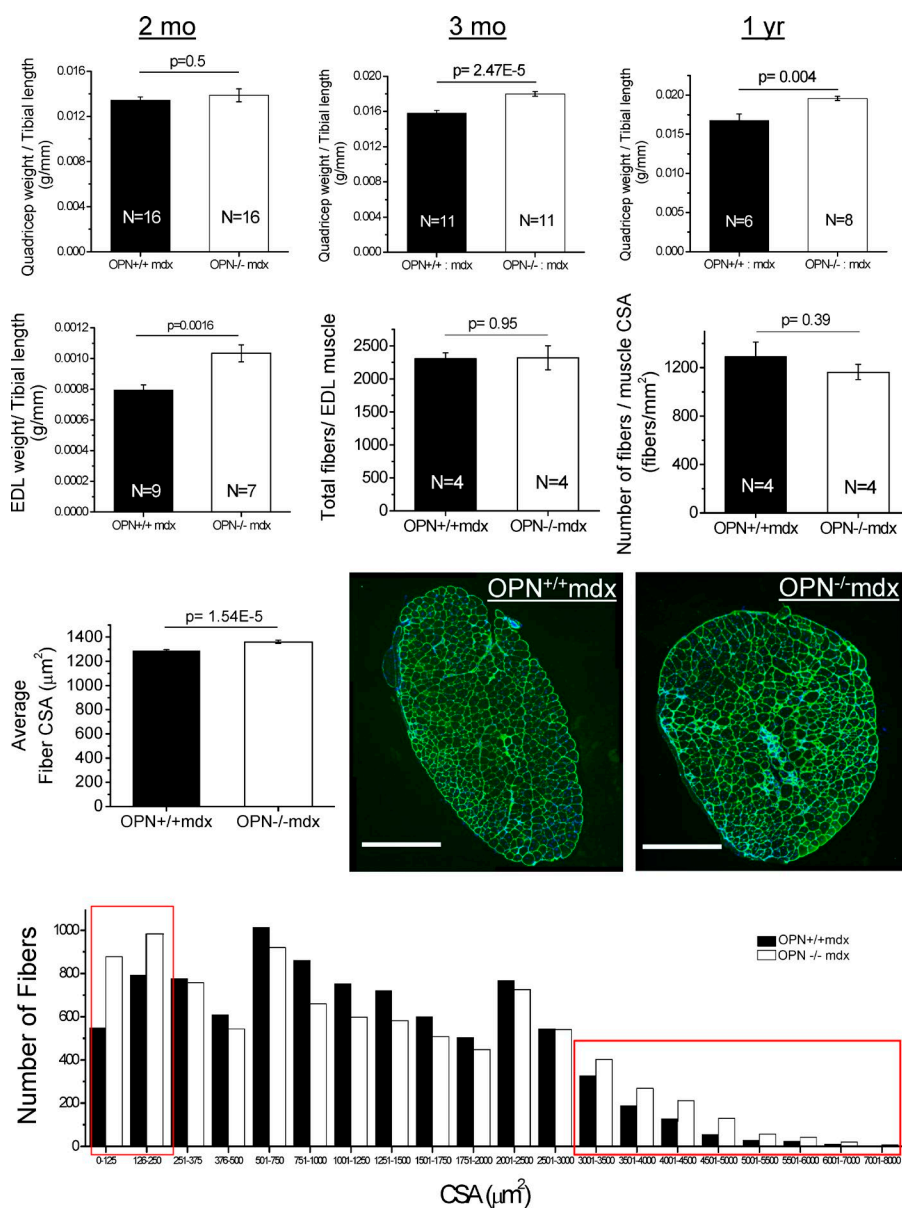
Figure 9. **OPN ablation leads to increased muscle mass and size.** The quadriceps and EDL muscles were evaluated for muscle mass at the ages indicated and data were normalized per tibial length. All cross sectional area and fiber analyses were conducted on the EDL. Vertical lines represent standard error. *, P < 0.05; #, P ≤ 0.02, determined by Student's *t* test. Bars, 500 µm. CSA, cross-sectional area. Average fiber cross-sectional area was calculated from *n* = >9,000 fibers per genotype per age.

et al., 2015). Studies in the dog model of DMD have demonstrated that levels of OPN correlate with degree of disability in different muscles (Galindo et al., 2015). Therefore, modulation of OPN has been demonstrated in mice, dogs, and humans to affect disease progression.

This study suggests that modulating immune cell infiltrates toward a more pro-regenerative phenotype may slow down disease progression and improve muscle function in the dystrophinopathies. Furthermore, it provides insight into OPN-mediated mechanisms of mdx dystrophy and supports the development of OPN inhibitors to treat DMD.

Materials and methods

Animals

C57BL/6J, mdx (C57BL/10ScSn-Dmd^{mdx}/J), and OPN-knockout mice (OPN-KO, B6.Cg-Spp1^{tm1Blh}/J) were obtained from the Jackson Laboratory. The mdx mice have a point mutation on exon 23 that generates a premature stop codon, leading to loss of expression of the full-length form of the dystrophin protein (Sicinski et al., 1989). On the other hand, OPN ablation in the OPN-KO mice was attained by replacing exons 4–7 of the *SPP1* gene with the phosphoglycerokinase neomycin resistance gene (Liaw et al., 1998). OPN$^{−/−}$mdx and OPN$^{+/+}$mdx mice came from colonies previously established in the laboratory (Vetrone et al., 2009) by breeding male OPN-KO mice with homozygous mdx females, which later resulted in OPN$^{+/−}$mdx mice that were crossed between them to obtain OPN$^{−/−}$mdx and OPN$^{+/+}$mdx mice. These colonies have been maintained in the University of California, Los Angeles (UCLA), vivarium by homozygous crosses. OPN$^{−/−}$mdx and OPN$^{+/+}$mdx colonies are in a mixed C57BL10/C57BL6 background with a predominance of the C57BL10 background (∼60% as determined by congenic analysis). All mice used in these experiments were genotyped using previously published protocols (Amalfitano and Chamberlain, 1996; Liaw et al., 1998) for the OPN and dystrophin mutations, respectively. All animals were handled and bred according to guidelines stipulated by the Animal Research Committee at UCLA.

Intramuscular cardiotoxin injection

Quadriceps muscles from 3-mo-old C57BL/6J and OPN-KO mice were injected once with 100 µl of a 10-µM cardiotoxin solution (CTX;
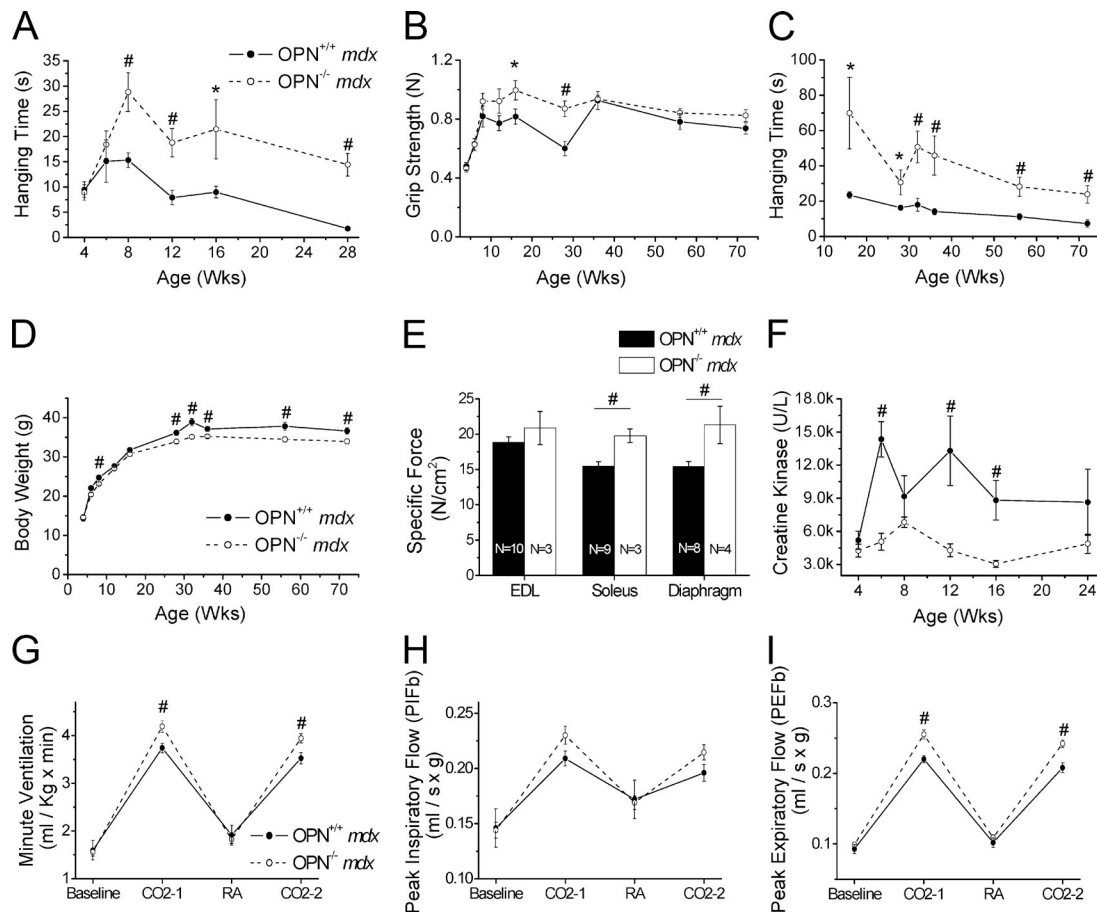
Figure 10. **Long-term improvements in muscle strength observed by functional and physiological testing of OPN$^{-/-}$mdx mice.** (A) Hanging wire test ($n = \geq 9$ per genotype and age). (B) Grip strength test ($n = \geq 9$ per genotype and age). (C) Wire mesh test ($n = \geq 10$ per genotype and age). (D) Body weight ($n = \geq 9$ per genotype and age). (E) Specific force (n indicated on bars of the graph). (F) Serum creatine kinase ($n = \geq 6$ per genotype and age). (G) Minute ventilation ($n = \geq 10$ per genotype and age). (H) Peak inspiratory flow ($n = \geq 10$ per genotype and age). (I) Peak expiratory flow ($n = \geq 10$ per genotype and age). Vertical lines represent standard error. *, $P < 0.05$; #, $P \leq 0.02$, determined by analysis of variance model.

cardiotoxin from *Naja mossambica mossambica*; Sigma-Aldrich) using a glass syringe (Hamilton Co.) with a 32-gauge needle (Hamilton Co.). CTX-injected muscles were dissected at 12, 24, 48, and 72 h after injection to be used for leukocyte isolation.

GM1 treatment of animals
Mdx mice were treated with an intraperitoneal injection of 30 µl of 1.1-mg polyclonal anti-asialo GM1 (CL8955; Cedarlane Laboratories) or polyclonal rabbit sera as a control (Invitrogen) twice a week. For all studies, injections began at 6 d of age and continued until mice reached 4 or 24 wk (6 mo) of age.

Wire test
Mice were tested by wire test as previously described (Vetrone et al., 2009). In brief, mice were placed on a wire secured 2 feet above a safety net and allowed to use forelimbs and hindlimbs (but not tails) to hang. Each mouse was subjected to five trials, with 1 min of rest between trials. Hang time was recorded from the moment the experimenter placed the mouse onto the wire until the mouse fell onto the safety net. The five data points were averaged and data expressed in seconds.

Grip strength
Forelimb grip strength was measured using a digital force gauge (DFIS 2; Chatillon CE). Five trials were performed with 30 s of rest in between. In each trial, the mouse was allowed to grasp a metal rod and

the technician slowly pulled the mouse by the tail until the digital gauge recorded the peak tension produced (in newtons [N]). Data are reported as a mean of the peak tension recorded in the five trials.

Wire mesh test
To assess overall muscle strength in vivo, mice were tested by wire mesh (custom built in the laboratory of M.J. Spencer). In brief, mice were placed in the center of a wire mesh pulled over a square wooden frame on a swivel. The apparatus was placed ~1.5 ft over a cushioned floor. Once the mouse was in position, the wire mesh was rotated 180°, resulting in the mouse hanging upside down from the mesh. Because of the structure of the mesh, mice were only able to hang on to the mesh using their hindlimb and forelimb paws. Hang time was recorded from the moment the experimenter began to rotate the mesh until the mouse fell off the mesh. Each mouse was subjected to five trials, with 1 min of rest between trials. The mean hang time across five trials was calculated for each mouse.

Isolated muscle mechanics
Muscle-specific force measurements from isolated EDL, soleus, and diaphragm muscles of 7-mo-old OPN$^{+/+}$mdx and OPN$^{-/-}$mdx mice were performed as previously described (Barton et al., 2010; Moorwood et al., 2013). In brief, mice were anesthetized with ketamine/xylazine and executed; muscles were removed and placed in a bath of Ringer's solution gas-equilibrated with 95% O_2/5% CO_2. Sutures were attached to the distal and proximal tendons of the EDL and soleus

muscles and to the central tendon and rib of the diaphragm preparations. Muscles were subjected to isolated mechanical measurements using a previously described device (Aurora Scientific; Barton et al., 2005) and bathed in Ringer's solution gas-equilibrated with 95% O_2/5% CO_2. After determining optimum length (Lo) by supramaximal twitch stimulation, maximum isometric tetanus was measured in the muscles during a 500-ms stimulation. Upon completion of these measurements, samples were rinsed in PBS, blotted, and weighed. Muscle cross-sectional areas were determined using the following formula: $CSA = m/(Lo \times L/Lo \times 1.06 \text{ g/cm}^3)$, where m is muscle mass, Lo is muscle length, L/Lo is the ratio of fiber length to muscle length, and 1.06 is the density of muscle.

Whole-body plethysmography

Respiratory function was measured in conscious, unrestrained mice using a whole-body plethysmograph (Buxco, Data Sciences International). In this system, mice are placed in a chamber that allows them to breathe naturally, unrestrained and untethered. The system measures the small changes in the air that is exchanged in and out of the entire chamber because of the animal's respiration (box flow). Each chamber was calibrated before every experiment, selecting the most appropriate response observed in FinePoint Software (Buxco, Data Sciences International) to the injection of 1 ml air into the chambers. Once all chambers were calibrated, mice were placed into chambers and allowed to acclimate for 55 min. A Bias Flow Regulator (Buxco, Data Sciences International) was used to prevent a rise in CO_2 concentration during the acclimation and room air breathing periods. After acclimation, baseline respiratory function was measured for 5 min. Subsequently, mice were subjected to two hypercapnic challenges in which a flow of 1 ml/min of 8% CO_2/21% O_2/balance N_2 (Praxair) was injected for 5 min into the chamber. Between the two hypercapnic challenges, mice were allowed to return to room air breathing for 10 min to evaluate their capability to recover. All data were collected and analyzed using FinePoint Software, which uses complicated algorithms that include variables affecting respiratory function, such as humidity and temperature, to calculate from the measured box flow the physiological values of the respiratory parameters from the animal. Mice were weighed before the beginning of the experiment. Minute ventilation and peak flow values were normalized to body weight.

Serum creatine kinase

Blood samples were collected by retroorbital puncture using heparinized capillary tubes and transferred to serum-separating tubes. Samples were kept at RT for 15 min to allow the blood to clot and then centrifuged at 3,400 g for 10 min to separate the serum. Once separated, serum was collected and stored at −80°C. Creatine kinase activity in blood was estimated using the Creatine Kinase-SL kit from Sekisui Diagnostics, according to the manufacturer's instructions. In brief, serum samples were diluted 1:50 (vol/vol) with sterile Ca^{2+},Mg^{2+}-free PBS. Controls for this test were established using the commercial control serums DC-TROL level-1 and level-2 (Sekisui Diagnostics). Samples and controls were set in triplicate in a 96-well plate and mixed with the reaction buffers provided in the kit. Absorbance of the samples was measured at 340 nm using a Synergy HT multidetection microplate reader (Biotek Instruments). Creatine kinase concentration was reported in units per liter and calculated using the following equation:

$$CK \text{ (U/L)} = \frac{\Delta Abs \times TV \times 1,000}{d \times \varepsilon \times SV},$$

where ΔAbs = mean absorbance change per minute; TV = total reaction volume (ml); d = light path (cm); ε = millimolar absorptivity of NADH (6.22); SV = sample volume (ml); and 1,000 = conversion of U/ml to U/l.

Muscle-infiltrating leukocyte isolation

Mice were sacrificed, and all muscles (hindlimb, pectoralis, diaphragm, and abdominal) from each mouse were collected and pooled together into a Petri dish containing sterile Ca^{2+},Mg^{2+}-free PBS. Tissues were washed twice with sterile Ca^{2+},Mg^{2+}-free PBS and then minced and digested into collagenase type 2 (Worthington Biochemical Corp.) solution (1,700 U/ml) at 37°C with slow agitation. Once the tissue was digested, the sample volume was raised with sterile Ca^{2+},Mg^{2+}-free PBS to stop the digestion and passed through a 70-μm cell strainer. Cells were pelleted by centrifugation of the filtered mix at 900 g for 5 min. Supernatant was discarded, and the pellet was resuspended in ammonium-chloride-potassium lysing buffer for 5 min to lyse the red blood cells. The lysing process was then stopped by raising the volume of the sample with sterile Ca^{2+},Mg^{2+}-free PBS, and the suspension was centrifuged at 900 g for 5 min to collect the cells. The cell pellet was suspended again in sterile Ca^{2+},Mg^{2+}-free PBS and passed through a 40-μm cell strainer. The filtered cell suspension was then centrifuged at 900 g for 5 min, the supernatant was discarded, and the cell pellet was resuspended in a small volume of sterile Ca^{2+},Mg^{2+}-free PBS. At this point, a small fraction of the sample was mixed 1:1 with 0.4% Trypan blue solution, and the number of unstained cells in the sample was counted using a hemocytometer. The concentration of viable cells in the sample and the total number of viable cells was then assessed using the following formulas: viable cells/ml = unstained number of cells × dilution factor × 10^4; total viable cells = viable cells/ml × final volume of the sample.

MACS of isolated macrophages

Macrophage isolation from the total leukocyte population was performed using Miltenyi Biotec MACS technology. Isolated intramuscular leukocyte samples were first blocked with an antibody against CD16/CD32 (anti-mouse, clone 93; Biolegend) to decrease nonspecific labeling and then stained with fluorescently labeled anti-F4/80 (rat anti-mouse, clone BM8, either PE- or APC-labeled; eBioscience). We used the company protocol for cell labeling and separation, with magnetic nanoparticles coated with antibodies against the fluorescent label used for the primary antibody (either anti-PE– or anti-APC–coated microbeads; Miltenyi Biotec).

FACS of isolated macrophages

MACS-sorted F4/80+ samples were labeled with fluorescently tagged antibodies against Ly6C (rat anti-mouse, Clone HK1.4; Biolegend), Siglec-F (rat anti-mouse, clone E50-2440; BD Biosciences), or their respective isotype controls (Rat IgG2c,K and Rat IgG2a,k, respectively). Fluorescently labeled samples were sorted using a FACScalibur (Becton Dickinson) flow cytometer. Acquisition parameters (voltage, gain, etc.) were adjusted with aliquots of the same samples to obtain the maximum dynamic range of SSC-H, FSC-H, and fluorescence (at the different channels). FACS acquisition files were analyzed using FlowJo analysis software.

Macrophage subtype isolation using FACS

Six 4-wk-old and six 8-wk-old OPN+/+mdx mice were used to isolated the individual macrophage subtype populations. Muscles (hindlimb, pectoralis, diaphragm, and abdominal) from all six mice were pooled together, and intramuscular leukocyte isolation was performed as described earlier. Isolated intramuscular leukocyte samples were first blocked with an antibody against CD16/CD32 (anti-mouse, clone 93; Biolegend) to decrease nonspecific labeling and then dually stained with anti-F4/80-APC (rat anti-mouse, clone BM8; eBioscience) and anti–Ly6C-FITC (rat anti-mouse, clone HK1.4; Biolegend). Fluorescently labeled samples were sorted using a FACSARIA III (Becton Dickinson). Unlabeled samples were used as control. Acquisition parameters

(voltage, gain, etc.) were adjusted with aliquots of the same samples to obtain the maximum dynamic range of SSC-H, FSC-H, and fluorescence (at the different channels). Macrophage population limits were established using gates resembling those of the analytical experiments.

Macrophage culture and polarization treatments

The murine monocyte/macrophage cell line J774A.1 (ATCC) was used as the in vitro macrophage model. Macrophages were grown and maintained in macrophage growth medium (DMEM, 1% penicillin/streptomycin, and 10% FBS), and subculture was prepared by scraping. Macrophage polarization was attained by incubation of the macrophage cultures with growth medium supplemented with 100 ng/ml murine IFNγ, IL-4, or IL-10 (BD) to polarize the cultures to M1, M2a, or M2c macrophages, respectively.

Isolation of liver NKT cells

Livers were removed and dissociated using the end of a 5-cc syringe plunger and a 70-µM cell strainer. Cell suspensions were centrifuged at 900 g for 6 min at RT. Cell pellets were resuspended in 0.85% ammonium chloride and incubated at RT for 10 min to lyse red blood cells. After incubation, suspensions were diluted with Dulbecco's PBS without Ca$^+$ and Mg$^+$ (Invitrogen) to stop the lysing process and centrifuged for 6 min at 900 g. Pellets were resuspended in 40% Percoll and loaded to the top of a Percoll gradient (70% Percoll at bottom and 40% at top). Tubes were then centrifuged at RT for 20 min at 2,000 rpm. The cells at the interface were collected and washed, and the resulting pellets were resuspended in PBS and counted.

Antibody staining for flow cytometry of NKT cells

Muscle leukocyte suspensions were incubated with anti-CD16/CD32 (anti-mouse, clone 2.4G2; BD) to block binding to Fc receptors before staining. The following mouse mAbs used for staining were all obtained from BD: CD3e (hamster anti-mouse, clone 145-2C11), Vβ8.1/8.2 (mouse anti-mouse, clone MR5-2), NK1.1 (mouse anti-mouse, clone PK136), and pan-NK (rat anti-mouse, clone DX5). Antibodies were conjugated to FITC, PE, and/or Cy5. The following antibodies were biotinylated and revealed with Tricolor-conjugated streptavidin (Ebioscience): anti–asialo-GM1 (CL8955; Cedarlane Laboratories) or rabbit sera (control; Invitrogen). Optimal working dilutions were determined for each antibody before use. All incubations were performed in Ca$^+$,Mg$^+$-free Dulbecco's PBS (Invitrogen) at 4°C for 30 min. After the last wash, 10^3 live cells per sample were acquired on a FACScalibur (Becton Dickinson) and analyzed with CELL Quest Pro software (Becton Dickinson). CD1d tetramers were obtained from the National Institutes of Health Tetramer Core Facility.

Immunohistochemistry

Muscles were dissected, placed on balsa wood, coated with Tissue Tek O.C.T. (optimal cutting temperature; Sakura Finetek) mounting media, and frozen in isopentane cooled by liquid nitrogen. Diaphragm muscles were cut in half down the midline and rolled before freezing. Sections were cut on a Micron HM 505E cryostat (10 µm thick; Micron Instruments) and stored at −20°C until use. Immunohistochemistry was performed as previously described (Kramerova et al., 2004). In brief, sections were thawed at RT for 30 min then treated with 0.3% H$_2$O$_2$ for 5 min and blocked in PBS with 0.2% gelatin, 0.5% Tween-20, and 3% BSA for 30 min. When necessary, binding to endogenous mouse IgG was blocked with a mouse on mouse kit (MOM; Vector Laboratories). Sections were later incubated with antibodies against T cell receptor Vα24 (eBioscience) to identify NKT cells in human biopsies, CD11b (clone M1/70; BD Biosciences) to emphasize areas of inflammation, or stained with neural cell adhesion molecule (NCAM; clone

H28.123; Chemicon International) or developmental myosin heavy chain (devMHC, clone RNMy2/9D2; Novacastra) to emphasize regenerating fibers. Biotin-conjugated antibodies (Vector Laboratories) were used as secondary antibodies, followed by incubation with avidin-conjugated horseradish peroxidase and staining with the AEC substrate kit (Vector Laboratories). To evaluate the cross-sectional area of muscles and fibers, muscle sections were immunolabeled with laminin antibodies. Sections were thawed at RT for 30 min, washed in PBS, blocked in PBS with 0.2% gelatin, 0.5% Tween-20, and 3% BSA for 30 min, incubated with anti-laminin antibody (L9393; Sigma-Aldrich) for 1 h, washed in PBS, and incubated with fluorescein anti-rabbit antibody (Vector Laboratories) for 1 h. Finally, sections were washed in PBS, fixed with 2% paraformaldehyde solution for 10 min, washed again in PBS, and mounted with DAPI mounting media (Vector Laboratories). Muscle sections were imaged using an Axio Imager M1 microscope (ZEISS) equipped with an AxioCam HRc camera (ZEISS). Mosaic images of the muscle sections were taken using a 10× EC Plan-NEO FLUAR objective (NA 0.3; ZEISS) and zoomed images were acquired using a 20× EC Plan-NEOFLUAR objective (NA 0.5; ZEISS). Images were acquired, processed, and analyzed using the proprietary software Axiovision 4.8.1 (ZEISS).

Histopathology index

Muscle necrosis was quantified from the muscle sections labeled with anti-CD11b antibody as the sum of the labeled (CD11b$^+$) areas in a section, normalized by the total cross-sectional area of the muscle section. Similarly, muscle regeneration was evaluated from the muscle sections labeled with anti-NCAM or anti-devMHC antibodies by counting the number of both small-diameter myotubes and large-diameter regenerating myofibers positively labeled with NCAM or devMHC, and normalizing this by the total cross-sectional area of the muscle. Cross-sectional areas were measured using Axiovision 4.8.1. All analyses were performed blindly.

Western blot

Cell culture samples were lysed in reducing sample buffer (50 mM Tris-HCl, pH 6.8, 10% glycerol, 2% SDS, and 100 mM β-mercaptoethanol) supplemented with protease and phosphatase inhibitors. Bromophenol blue (0.1%) was added, and samples were boiled at 100°C for 5 min for protein denaturation. SDS-PAGE and Western blotting were performed as previously described (Kramerova et al., 2004). BenchMark protein ladder was used as a molecular weight marker in every gel. Proteins were separated by gel electrophoresis and transferred into a nitrocellulose membrane. Membranes were blocked with 5% milk in TBS-T (Tris-buffered saline, 0.1% Tween) and incubated with 1:500 anti-mouse OPN antibody (AF808; R&D Systems) solution in 5% milk TBS-T overnight at 4°C. Membranes were washed and incubated with HRP-conjugated secondary antibody in 5% milk TBS-T. The chemiluminescence substrate kit, ChemiGlow West (Protein Simple), was used to detect the protein bands. Chemiluminescent signals were detected and densitometry analyzed using the FluorChem FC2 system (Alpha Innotech).

Quantitative RT-PCR

RNA was isolated and quantitative RT-PCR performed as previously described (Ermolova et al., 2014). In brief, total RNA was isolated from cell cultures and isolated cells using Trizol reagent (Invitrogen) according to the manufacturer's protocol. Genomic DNA contamination was removed by DNase I treatment (Invitrogen). To synthesize cDNA, 1.5 µg of DNA-free RNA was used for first-strand cDNA synthesis with random hexamer primers and Superscript III reverse transcription (Invitrogen) according to the company's protocol. The resulting

cDNAs were used for PCR amplification using the primers sequences detailed in Table S2. Quantitative PCR reaction was set using the iTaq universal SYBR green supermix (Bio-Rad) according to the manufacturer's protocol. PCR product formation was evaluated using the CFX-Connect Real Time System (Bio-Rad).

Statistical analysis

Means were compared by genotype and age using a factorial analysis of variance model in which variances were allowed to be heterogeneous, since variance homogeneity did not hold. For pulmonary outcomes in which the same animal was exposed to CO_2 and room air conditions, means were compared by genotype and condition using a repeated-measure analysis of variance model (mixed model). Post hoc (under the model) p-values were computed using the Fisher least significant difference criterion. Residual error normal quartile plots were examined to confirm that the residual errors followed a normal distribution, allowing the use of a parametric model. Student's t test or Mann–Whitney U test were used for experiments using only two groups. Values were considered significantly different if $P \leq 0.05$.

Online supplemental material

Fig. S1 shows the effect of OPN ablation on macrophage polarization in acute injury experiments (CTX injection experiments). Fig. S2 provides information about the degree of improvement caused by OPN ablation in mdx mice by comparing the performance of C57BL/6J and OPN$^{-/-}$mdx mice in different muscle strength tests. Table S1 provides the total cell number in the different macrophage subtypes per muscle mass, from the experiments shown in Fig. 4 for 8-wk-old mice. Table S2 summarizes the sequences of the primers used. Online supplemental material is available at http://www.jcb.org/cgi/content/full/jcb.201510086/DC1.

References

Amalfitano, A., and J.S. Chamberlain. 1996. The mdx-amplification-resistant mutation system assay, a simple and rapid polymerase chain reaction-based detection of the mdx allele. *Muscle Nerve.* 19:1549–1553. http://dx.doi.org/10.1002/(SICI)1097-4598(199612)19:12<1549::AID-MUS4>3.0.CO;2-A

Arnold, L., A. Henry, F. Poron, Y. Baba-Amer, N. van Rooijen, A. Plonquet, R.K. Gherardi, and B. Chazaud. 2007. Inflammatory monocytes recruited after skeletal muscle injury switch into antiinflammatory macrophages to support myogenesis. *J. Exp. Med.* 204:1057–1069. http://dx.doi.org/10.1084/jem.20070075

Ashkar, S., G.F. Weber, V. Panoutsakopoulou, M.E. Sanchirico, M. Jansson, S. Zawaideh, S.R. Rittling, D.T. Denhardt, M.J. Glimcher, and H. Cantor. 2000. Eta-1 (osteopontin): An early component of type-1 (cell-mediated) immunity. *Science.* 287:860–864. http://dx.doi.org/10.1126/science.287.5454.860

Barton, E.R., L. Morris, A. Musaro, N. Rosenthal, and H.L. Sweeney. 2002. Muscle-specific expression of insulin-like growth factor I counters muscle decline in mdx mice. *J. Cell Biol.* 157:137–148. http://dx.doi.org/10.1083/jcb.200108071

Barton, E.R., L. Morris, M. Kawana, L.T. Bish, and T. Toursel. 2005. Systemic administration of L-arginine benefits mdx skeletal muscle function. *Muscle Nerve.* 32:751–760. http://dx.doi.org/10.1002/mus.20425

Barton, E.R., B.J. Wang, B.K. Brisson, and H.L. Sweeney. 2010. Diaphragm displays early and progressive functional deficits in dysferlin-deficient mice. *Muscle Nerve.* 42:22–29. http://dx.doi.org/10.1002/mus.21645

Bayless, K.J., G.A. Meininger, J.M. Scholtz, and G.E. Davis. 1998. Osteopontin is a ligand for the alpha4beta1 integrin. *J. Cell Sci.* 111:1165–1174.

Bello, L., A. Kesari, H. Gordish-Dressman, A. Cnaan, L.P. Morgenroth, J. Punetha, T. Duong, E.K. Henricson, E. Pegoraro, C.M. McDonald, and E.P. Hoffman. Cooperative International Neuromuscular Research Group Investigators. 2015. Genetic modifiers of ambulation in the Cooperative International Neuromuscular Research Group Duchenne Natural History Study. *Ann. Neurol.* 77:684–696. http://dx.doi.org/10.1002/ana.24370

Belperio, J.A., M. Dy, L. Murray, M.D. Burdick, Y.Y. Xue, R.M. Strieter, and M.P. Keane. 2004. The role of the Th2 CC chemokine ligand CCL17 in pulmonary fibrosis. *J. Immunol.* 173:4692–4698. http://dx.doi.org/10.4049/jimmunol.173.7.4692

Borthwick, L.A., T.A. Wynn, and A.J. Fisher. 2013. Cytokine mediated tissue fibrosis. *Biochim. Biophys. Acta.* 1832:1049–1060. http://dx.doi.org/10.1016/j.bbadis.2012.09.014

Bryer, S.C., G. Fantuzzi, N. Van Rooijen, and T.J. Koh. 2008. Urokinase-type plasminogen activator plays essential roles in macrophage chemotaxis and skeletal muscle regeneration. *J. Immunol.* 180:1179–1188. http://dx.doi.org/10.4049/jimmunol.180.2.1179

Bushby, K., R. Finkel, D.J. Birnkrant, L.E. Case, P.R. Clemens, L. Cripe, A. Kaul, K. Kinnett, C. McDonald, S. Pandya, et al. DMD Care Considerations Working Group. 2010. Diagnosis and management of Duchenne muscular dystrophy, part 1: Diagnosis, and pharmacological and psychosocial management. *Lancet Neurol.* 9:77–93. http://dx.doi.org/10.1016/S1474-4422(09)70271-6

Byrne, P., P. McGuirk, S. Todryk, and K.H. Mills. 2004. Depletion of NK cells results in disseminating lethal infection with *Bordetella pertussis* associated with a reduction of antigen-specific Th1 and enhancement of Th2, but not Tr1, cells. *Eur. J. Immunol.* 34:2579–2588. http://dx.doi.org/10.1002/eji.200425092

Cantini, M., E. Giurisato, C. Radu, S. Tiozzo, F. Pampinella, D. Senigaglia, G. Zaniolo, F. Mazzoleni, and L. Vitiello. 2002. Macrophage-secreted myogenic factors: A promising tool for greatly enhancing the proliferative capacity of myoblasts in vitro and in vivo. *Neurol. Sci.* 23:189–194. http://dx.doi.org/10.1007/s100720200060

Casals, G., J. Ordi, M. Creus, F. Fábregues, R. Casamitjana, L. Quinto, E. Campo, and J. Balasch. 2008. Osteopontin and alphavbeta3 integrin expression in the endometrium of infertile and fertile women. *Reprod. Biomed. Online.* 16:808–816. http://dx.doi.org/10.1016/S1472-6483(10)60146-0

Crane, M.J., J.M. Daley, O. van Houtte, S.K. Brancato, W.L. Henry Jr., and J.E. Albina. 2014. The monocyte to macrophage transition in the murine sterile wound. *PLoS One.* 9:e86660. http://dx.doi.org/10.1371/journal.pone.0086660

Das, R., S. Philip, G.H. Mahabeleshwar, A. Bulbule, and G.C. Kundu. 2005. Osteopontin: Its role in regulation of cell motility and nuclear factor kappa B-mediated urokinase type plasminogen activator expression. *IUBMB Life.* 57:441–447. http://dx.doi.org/10.1080/15216540500159424

Dumont, N., and J. Frenette. 2010. Macrophages protect against muscle atrophy and promote muscle recovery in vivo and in vitro: A mechanism partly dependent on the insulin-like growth factor-1 signaling molecule. *Am. J. Pathol.* 176:2228–2235. http://dx.doi.org/10.2353/ajpath.2010.090884

Ermolova, N.V., L. Martinez, S.A. Vetrone, M.C. Jordan, K.P. Roos, H.L. Sweeney, and M.J. Spencer. 2014. Long-term administration of the TNF blocking drug Remicade (cV1q) to mdx mice reduces skeletal and cardiac muscle fibrosis, but negatively impacts cardiac function. *Neuromuscul. Disord.* 24:583–595. http://dx.doi.org/10.1016/j.nmd.2014.04.006

Galindo, C.L., J.H. Soslow, C.L. Brinkmeyer-Langford, M. Gupte, H.M. Smith, S. Sengsayadeth, D.B. Sawyer, D.W. Benson, J.N. Kornegay, and L.W. Markham. 2015. Translating golden retriever muscular dystrophy microarray findings to novel biomarkers for cardiac/skeletal muscle function in Duchenne muscular dystrophy. *Pediatr. Res.* http://dx.doi.org/10.1038/pr.2015.257

Gao, C., H. Guo, Z. Mi, M.J. Grusby, and P.C. Kuo. 2007. Osteopontin induces ubiquitin-dependent degradation of STAT1 in RAW264.7 murine macrophages. *J. Immunol.* 178:1870–1881. http://dx.doi.org/10.4049/jimmunol.178.3.1870

Godfrey, D.I., and M. Kronenberg. 2004. Going both ways: Immune regulation via CD1d-dependent NKT cells. *J. Clin. Invest.* 114:1379–1388. http://dx.doi.org/10.1172/JCI200423594

Goodison, S., V. Urquidi, and D. Tarin. 1999. CD44 cell adhesion molecules. *MP, Mol. Pathol.* 52:189–196. http://dx.doi.org/10.1136/mp.52.4.189

Haslett, J.N., D. Sanoudou, A.T. Kho, R.R. Bennett, S.A. Greenberg, I.S. Kohane, A.H. Beggs, and L.M. Kunkel. 2002. Gene expression comparison of biopsies from Duchenne muscular dystrophy (DMD) and normal skeletal muscle. *Proc. Natl. Acad. Sci. USA.* 99:15000–15005. http://dx.doi.org/10.1073/pnas.192571199

Heydemann, A., E. Ceco, J.E. Lim, M. Hadhazy, P. Ryder, J.L. Moran, D.R. Beier, A.A. Palmer, and E.M. McNally. 2009. Latent TGF-beta-binding protein 4 modifies muscular dystrophy in mice. *J. Clin. Invest.* 119:3703–3712. http://dx.doi.org/10.1172/JCI39845

Hunt, L.C., A. Upadhyay, J.A. Jazayeri, E.M. Tudor, and J.D. White. 2013. An anti-inflammatory role for leukemia inhibitory factor receptor signaling in regenerating skeletal muscle. *Histochem. Cell Biol.* 139:13–34. http://dx.doi.org/10.1007/s00418-012-1018-0

Kahles, F., H.M. Findeisen, and D. Bruemmer. 2014. Osteopontin: A novel regulator at the cross roads of inflammation, obesity and diabetes. *Mol. Metab.* 3:384–393. http://dx.doi.org/10.1016/j.molmet.2014.03.004

Koguchi, Y., K. Kawakami, S. Kon, T. Segawa, M. Maeda, T. Uede, and A. Saito. 2002. *Penicillium marneffei* causes osteopontin-mediated production of interleukin-12 by peripheral blood mononuclear cells. *Infect. Immun.* 70:1042–1048. http://dx.doi.org/10.1128/IAI.70.3.1042-1048.2002

Kramerova, I., E. Kudryashova, J.G. Tidball, and M.J. Spencer. 2004. Null mutation of calpain 3 (p94) in mice causes abnormal sarcomere formation in vivo and in vitro. *Hum. Mol. Genet.* 13:1373–1388. http://dx.doi.org/10.1093/hmg/ddh153

Kyriakides, T., E. Pegoraro, E.P. Hoffman, L. Piva, S. Cagnin, G. Lanfranchi, R.C. Griggs, and S.F. Nelson. 2011. SPP1 genotype is a determinant of disease severity in Duchenne muscular dystrophy: Predicting the severity of Duchenne muscular dystrophy: Implications for treatment. *Neurology.* 77:1858–1859. http://dx.doi.org/10.1212/WNL.0b013e318239b9ae

Liaw, L., D.E. Birk, C.B. Ballas, J.S. Whitsitt, J.M. Davidson, and B.L. Hogan. 1998. Altered wound healing in mice lacking a functional osteopontin gene (spp1). *J. Clin. Invest.* 101:1468–1478. http://dx.doi.org/10.1172/JCI2131

Liu, Y.C., X.B. Zou, Y.F. Chai, and Y.M. Yao. 2014. Macrophage polarization in inflammatory diseases. *Int. J. Biol. Sci.* 10:520–529. http://dx.doi.org/10.7150/ijbs.8879

Mann, C.J., E. Perdiguero, Y. Kharraz, S. Aguilar, P. Pessina, A.L. Serrano, and P. Muñoz-Cánoves. 2011. Aberrant repair and fibrosis development in skeletal muscle. *Skelet. Muscle.* 1:21. http://dx.doi.org/10.1186/2044-5040-1-21

Mantovani, A., A. Sica, and M. Locati. 2007. New vistas on macrophage differentiation and activation. *Eur. J. Immunol.* 37:14–16. http://dx.doi.org/10.1002/eji.200636910

McDouall, R.M., M.J. Dunn, and V. Dubowitz. 1990. Nature of the mononuclear infiltrate and the mechanism of muscle damage in juvenile dermatomyositis and Duchenne muscular dystrophy. *J. Neurol. Sci.* 99:199–217. http://dx.doi.org/10.1016/0022-510X(90)90156-H

Mojumdar, K., F. Liang, C. Giordano, C. Lemaire, G. Danialou, T. Okazaki, J. Bourdon, M. Rafei, J. Galipeau, M. Divangahi, and B.J. Petrof. 2014. Inflammatory monocytes promote progression of Duchenne muscular dystrophy and can be therapeutically targeted via CCR2. *EMBO Mol. Med.* 6:1476–1492. http://dx.doi.org/10.15252/emmm.201403967

Moorwood, C., M. Liu, Z. Tian, and E.R. Barton. 2013. Isometric and eccentric force generation assessment of skeletal muscles isolated from murine models of muscular dystrophies. *J. Vis. Exp.* (71):e50036. http://dx.doi.org/10.3791/50036

Nakagawa, R., I. Nagafune, Y. Tazunoki, H. Ehara, H. Tomura, R. Iijima, K. Motoki, M. Kamishohara, and S. Seki. 2001. Mechanisms of the antimetastatic effect in the liver and of the hepatocyte injury induced by alpha-galactosylceramide in mice. *J. Immunol.* 166:6578–6584. http://dx.doi.org/10.4049/jimmunol.166.11.6578

Nakano, Y., H. Hisaeda, T. Sakai, H. Ishikawa, M. Zhang, T. Maekawa, T. Zhang, M. Takashima, M. Nishitani, R.A. Good, and K. Himeno. 2002. Roles of NKT cells in resistance against infection with *Toxoplasma gondii* and in expression of heat shock protein 65 in the host macrophages. *Microbes Infect.* 4:1–11. http://dx.doi.org/10.1016/S1286-4579(01)01503-9

Naldini, A., D. Leali, A. Pucci, E. Morena, F. Carraro, B. Nico, D. Ribatti, and M. Presta. 2006. Cutting edge: IL-1beta mediates the proangiogenic activity of osteopontin-activated human monocytes. *J. Immunol.* 177:4267–4270. http://dx.doi.org/10.4049/jimmunol.177.7.4267

Novak, M.L., and T.J. Koh. 2013. Macrophage phenotypes during tissue repair. *J. Leukoc. Biol.* 93:875–881. http://dx.doi.org/10.1189/jlb.1012512

Nyström, T., P. Dunér, and A. Hultgårdh-Nilsson. 2007. A constitutive endogenous osteopontin production is important for macrophage function and differentiation. *Exp. Cell Res.* 313:1149–1160. http://dx.doi.org/10.1016/j.yexcr.2006.12.026

Porter, J.D., S. Khanna, H.J. Kaminski, J.S. Rao, A.P. Merriam, C.R. Richmonds, P. Leahy, J. Li, W. Guo, and F.H. Andrade. 2002. A chronic inflammatory response dominates the skeletal muscle molecular signature in dystrophin-deficient mdx mice. *Hum. Mol. Genet.* 11:263–272. http://dx.doi.org/10.1093/hmg/11.3.263

Rigamonti, E., P. Zordan, C. Sciorati, P. Rovere-Querini, and S. Brunelli. 2014. Macrophage plasticity in skeletal muscle repair. *BioMed Res. Int.* 2014:560629. http://dx.doi.org/10.1155/2014/560629

Rollo, E.E., and D.T. Denhardt. 1996. Differential effects of osteopontin on the cytotoxic activity of macrophages from young and old mice. *Immunology.* 88:642–647. http://dx.doi.org/10.1046/j.1365-2567.1996.d01-691.x

Rollo, E.E., D.L. Laskin, and D.T. Denhardt. 1996. Osteopontin inhibits nitric oxide production and cytotoxicity by activated RAW264.7 macrophages. *J. Leukoc. Biol.* 60:397–404.

Saclier, M., H. Yacoub-Youssef, A.L. Mackey, L. Arnold, H. Ardjoune, M. Magnan, F. Sailhan, J. Chelly, G.K. Pavlath, R. Mounier, et al. 2013. Differentially activated macrophages orchestrate myogenic precursor cell fate during human skeletal muscle regeneration. *Stem Cells.* 31:384–396. http://dx.doi.org/10.1002/stem.1288

Sicinski, P., Y. Geng, A.S. Ryder-Cook, E.A. Barnard, M.G. Darlison, and P.J. Barnard. 1989. The molecular basis of muscular dystrophy in the mdx mouse: a point mutation. *Science.* 244:1578–1580. http://dx.doi.org/10.1126/science.2662404

Slifka, M.K., R.R. Pagarigan, and J.L. Whitton. 2000. NK markers are expressed on a high percentage of virus-specific CD8+ and CD4+ T cells. *J. Immunol.* 164:2009–2015. http://dx.doi.org/10.4049/jimmunol.164.4.2009

Song, E., N. Ouyang, M. Hörbelt, B. Antus, M. Wang, and M.S. Exton. 2000. Influence of alternatively and classically activated macrophages on fibrogenic activities of human fibroblasts. *Cell. Immunol.* 204:19–28. http://dx.doi.org/10.1006/cimm.2000.1687

Suelves, M., B. Vidal, A.L. Serrano, M. Tjwa, J. Roma, R. López-Alemany, A. Luttun, M.M. de Lagrán, A. Díaz-Ramos, M. Jardí, et al. 2007. uPA deficiency exacerbates muscular dystrophy in MDX mice. *J. Cell Biol.* 178:1039–1051. http://dx.doi.org/10.1083/jcb.200705127

To, W.S., and K.S. Midwood. 2011. Plasma and cellular fibronectin: Distinct and independent functions during tissue repair. *Fibrogenesis Tissue Repair.* 4:21. http://dx.doi.org/10.1186/1755-1536-4-21

Varga, T., R. Mounier, P. Gogolak, S. Poliska, B. Chazaud, and L. Nagy. 2013. Tissue LyC6- macrophages are generated in the absence of circulating LyC6- monocytes and Nur77 in a model of muscle regeneration. *J. Immunol.* 191:5695–5701. http://dx.doi.org/10.4049/jimmunol.1301445

Vetrone, S.A., E. Montecino-Rodriguez, E. Kudryashova, I. Kramerova, E.P. Hoffman, S.D. Liu, M.C. Miceli, and M.J. Spencer. 2009. Osteopontin promotes fibrosis in dystrophic mouse muscle by modulating immune cell subsets and intramuscular TGF-beta. *J. Clin. Invest.* 119:1583–1594. http://dx.doi.org/10.1172/JCI37662

Vidal, B., A.L. Serrano, M. Tjwa, M. Suelves, E. Ardite, R. De Mori, B. Baeza-Raja, M. Martínez de Lagrán, P. Lafuste, V. Ruiz-Bonilla, et al. 2008. Fibrinogen drives dystrophic muscle fibrosis via a TGFbeta/alternative macrophage activation pathway. *Genes Dev.* 22:1747–1752. http://dx.doi.org/10.1101/gad.465908

Villalta, S.A., H.X. Nguyen, B. Deng, T. Gotoh, and J.G. Tidball. 2009. Shifts in macrophage phenotypes and macrophage competition for arginine metabolism affect the severity of muscle pathology in muscular dystrophy. *Hum. Mol. Genet.* 18:482–496. http://dx.doi.org/10.1093/hmg/ddn376

Villalta, S.A., B. Deng, C. Rinaldi, M. Wehling-Henricks, and J.G. Tidball. 2011a. IFN-γ promotes muscle damage in the mdx mouse model of Duchenne muscular dystrophy by suppressing M2 macrophage activation and inhibiting muscle cell proliferation. *J. Immunol.* 187:5419–5428. http://dx.doi.org/10.4049/jimmunol.1101267

Villalta, S.A., C. Rinaldi, B. Deng, G. Liu, B. Fedor, and J.G. Tidball. 2011b. Interleukin-10 reduces the pathology of mdx muscular dystrophy by deactivating M1 macrophages and modulating macrophage phenotype. *Hum. Mol. Genet.* 20:790–805. http://dx.doi.org/10.1093/hmg/ddq523

Weber, G.F., S. Zawaideh, S. Hikita, V.A. Kumar, H. Cantor, and S. Ashkar. 2002. Phosphorylation-dependent interaction of osteopontin with its receptors regulates macrophage migration and activation. *J. Leukoc. Biol.* 72:752–761.

Wehling, M., M.J. Spencer, and J.G. Tidball. 2001. A nitric oxide synthase transgene ameliorates muscular dystrophy in mdx mice. *J. Cell Biol.* 155:123–131. http://dx.doi.org/10.1083/jcb.200105110

Wermuth, P.J., and S.A. Jimenez. 2015. The significance of macrophage polarization subtypes for animal models of tissue fibrosis and human fibrotic diseases. *Clin. Transl. Med.* 4:2. http://dx.doi.org/10.1186/s40169-015-0047-4

Yogo, Y., S. Fujishima, T. Inoue, F. Saito, T. Shiomi, K. Yamaguchi, and A. Ishizaka. 2009. Macrophage derived chemokine (CCL22), thymus and activation-regulated chemokine (CCL17), and CCR4 in idiopathic pulmonary fibrosis. *Respir. Res.* 10:80. http://dx.doi.org/10.1186/1465-9921-10-80